AGU PUBLICATIONS

JGR

Journal of Geophysical Research: Space Physics

RESEARCH ARTICLE

10.1002/2014JA020374

Special Section:
New perspectives on Earth's radiation belt regions from the prime mission of the Van Allen Probes

Key Points:
- We report initial observations of ring current ions
- We show that He-ion decay rates are consistent with theory
- We show that O-ions with energies greater than 500 keV decay very rapidly

Correspondence to:
A. Gerrard,
gerrard@njit.edu

Citation:
Gerrard, A., L. Lanzerotti, M. Gkioulidou, D. Mitchell, J. Manweiler, J. Bortnik, and K. Keika (2014), Initial measurements of O-ion and He-ion decay rates observed from the Van Allen Probes RBSPICE instrument, *J. Geophys. Res. Space Physics*, *119*, 8813–8819, doi:10.1002/2014JA020374.

Received 7 JUL 2014
Accepted 6 OCT 2014
Accepted article online 8 OCT 2014
Published online 5 NOV 2014

Initial measurements of O-ion and He-ion decay rates observed from the Van Allen probes RBSPICE instrument

Andrew Gerrard[1], Louis Lanzerotti[1], Matina Gkioulidou[2], Donald Mitchell[2], Jerry Manweiler[3], Jacob Bortnik[4], and Kunihiro Keika[5]

[1]Center for Solar-Terrestrial Research, New Jersey Institute of Technology, Newark, New Jersey, USA, [2]John Hopkins University-Applied Physics Laboratory, Laurel, Maryland, USA, [3]Fundamental Technologies, LLC, Lawrence, Kansas, USA, [4]Department of Atmospheric and Oceanic Sciences, University of California, Los Angeles, California, USA, [5]Solar-Terrestrial Environment Laboratory, Nagoya University, Nagoya, Japan

Abstract H-ion (~45 keV to ~600 keV), He-ion (~65 keV to ~520 keV), and O-ion (~140 keV to ~1130 keV) integral flux measurements, from the Radiation Belt Storm Probe Ion Composition Experiment (RBSPICE) instrument aboard the Van Allan Probes spacecraft B, are reported. These abundance data form a cohesive picture of ring current ions during the first 9 months of measurements. Furthermore, the data presented herein are used to show injection characteristics via the He-ion/H-ion abundance ratio and the O-ion/H-ion abundance ratio. Of unique interest to ring current dynamics are the spatial-temporal decay characteristics of the two injected populations. We observe that He-ions decay more quickly at lower L shells, on the order of ~0.8 day at L shells of 3–4, and decay more slowly with higher L shell, on the order of ~1.7 days at L shells of 5–6. Conversely, O-ions decay very rapidly (~1.5 h) across all L shells. The He-ion decay time are consistent with previously measured and calculated lifetimes associated with charge exchange. The O-ion decay time is much faster than predicted and is attributed to the inclusion of higher-energy (> 500 keV) O-ions in our decay rate estimation. We note that these measurements demonstrate a compelling need for calculation of high-energy O-ion loss rates, which have not been adequately studied in the literature to date.

1. Introduction

Measurements by the Radiation Belt Storm Probes Ion Composition Experiment (RBSPICE) instrument [*Mitchell et al.*, 2013] provide the opportunity to examine the compositional changes of the Earth's ring current (i.e., energy greater than 10 keV and less than 1 MeV) during geomagnetically disturbed times. These measurements on the Van Allen Probes are the first long-term sets of composition data since the early 1990s that have been made in the inner magnetosphere near the geomagnetic equator and thus can define the magnetospheric response and the compositional changes in the particle energy range that make up ring current populations [*Mauk et al.*, 2012].

Systematic studies of inner magnetospheric H-ion, He-ion, and O-ion ring current abundances and their variations during quiet and moderately active times are relatively scarce, e.g., on Active Magnetosphere Particle Tracer Explorer/CCE [*Daglis et al.*, 1993; *Sheldon and Hamilton*, 1993] and CRRES/magnetospheric ion composition spectrometer [*Fu et al.*, 2001, 2003]. Though an extensive literature exists on the composition of the ring current and higher-energy trapped particle populations during geomagnetic storm conditions (e.g., review by *Keika et al.* [2013] and papers therein), it is difficult to find absolute flux measurements in these particular energy ranges (e.g., review by *Daglis et al.* [1999] and papers therein). Similarly, reports of He-ion/H-ion abundance ratios (i.e., hereafter the He/H ratio) and O-ion/H-ion abundance ratios (i.e., hereafter the O/H ratio) are likewise scarce at these energy ranges [e.g., *Krimigis and Van Allen*, 1967; *Fritz and Krimigis*, 1969; *Konradi et al.*, 1973; *Gloeckler et al.*, 1985; *Hamilton et al.*, 1988; *Kistler et al.*, 1989; *Fu et al.*, 2001; *Pulkkinen et al.*, 2001; *Fu et al.*, 2003; *Kronberg et al.*, 2012].

Of unique interest in contemporary ring current studies is the physical nature of loss mechanisms. Coulomb interactions (i.e., drag and scattering), charge exchange, drift/convective loss, and wave-particle interactions all play a role in particle loss, with each mechanism being present or even dominant at particular particle energies, particular particle masses, or particular spatial locations [*Ebihara and Ejiri*, 2003]. Between 50 and 1000 keV, the dominant loss mechanism present for ring current ions is likely charge exchange.

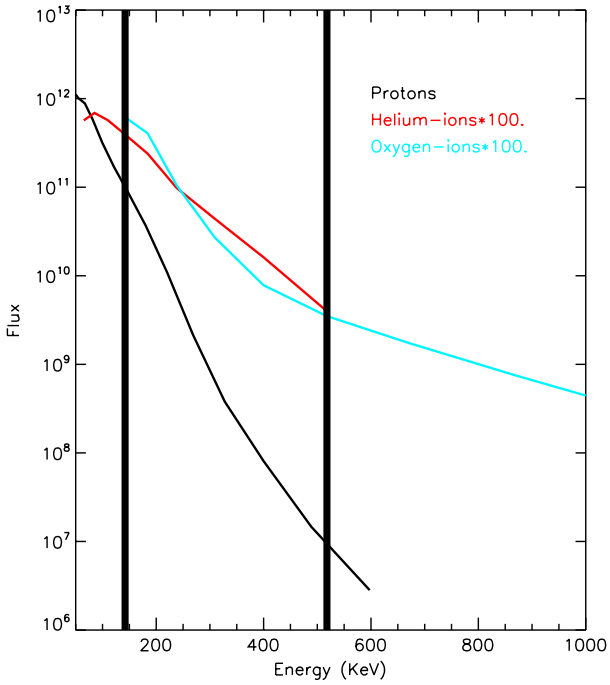

Figure 1. RBSPICE energy ranges for the protons (black trace), He-ions (red trace), and O-ions (blue trace), along with typical integrated flux values (particles/(s cm^2 keV)) at a dipole L shell of 5.5. He-ion and O-ion flux values are multiplied by 100 for comparative purposes. The vertical bars indicate the region of common energies, ~140 keV to ~520 keV.

In this paper H-ion (~45 keV to ~600 keV), He-ion (~65 keV to ~520 keV), and O-ion (~140 keV to ~1130 keV) abundance results from the RBSPICE instrument, all from Van Allan Probes spacecraft B, are reported. These abundance values are used to show injection (i.e., sudden transport into the inner magnetosphere) and loss characteristics via the He/H ratio and O/H ratio values. We pay particular attention to the observation of a rapid O/H ratio decay which has not been previously reported and does not fit the expected charge exchange paradigm.

2. Observations

Measurements of H-ion, He-ion, and O-ion fluxes are derived from the time of flight and total energy capabilities of the RBSPICE instrument [*Mitchell et al.*, 2013]. Specifically, ion velocities are determined by measuring the flight time of the particle between collisions with an entrance and exit foil. Each foil collision generates secondary electrons which are time-stamped by a microchannel plate. After passing through the last foil, the ion's total energy is determined by a solid-state detector. Six such independent channels (i.e., "telescopes," or independent fields-of-view) exist on the RBSPICE instrument which, when combined with the spin of the spacecraft, give full pitch angle coverage.

The fluxes reported herein are integrated over all pitch angles and over the total energy ranges quoted above. This was done so as to explore the full species flux, which has relevance to the *Dst* index value and solar wind influx. Figure 1 shows the species energy ranges and typical fluxes (particles/(s cm^2 keV)) at a dipole L shell ~5.5. We note that He-ions are largely composed of He^+, though some He^{+2} could be present in the most extreme of storm events. The presence of He^{+2} should not be an issue herein, given the fast rate of conversion of He^{+2} to He^+. O-ions are expected to be all O^+. All measurements shown here are well above the instrument noise floor and are statistically significant, as based on Poisson counting statistics.

In Figure 2 we show the measured H-ion, He-ion, and O-ion fluxes (particles/(s cm^2)) as functions of time and dipole L shell during the first nine mission months following commissioning of the RBSPICE instrument. These fluxes are obtained using 30 min duration and 0.1 dipole L shell binned data realizations. We note that such temporal bins smear-enhanced flux values often observed during injection events which can occur on the timescale of minutes. We also note that the RBSPICE instrument was shut off below L ~3 to reduce anomalous currents and instrument alarming. The hourly *Dst* index is plotted in the top panel for reference. During the time interval shown in Figure 2, the apogee of the Van Allen Probes precessed from ~6 magnetic local time (MLT) to ~17 MLT (i.e., from the dawnside, through the night, and toward the duskside) near the equatorial plane. Figure 3 shows four orbit snapshots in the GSE coordinate system over the time span of Figure 2.

Inspection of the data in Figure 2 shows a number of interesting features. Most clearly observed is the enhancement of the flux across all ionic species during active periods, as measured by drops in the *Dst* (e.g., on day of year 18, 28, 76, 120, and 150). This correlation with *Dst* is not unexpected, as the *Dst* is fundamentally a measure of the ring current to which these particles make up. More intriguing is the morphology of the injections in time and L shell. Such characteristics are best observed via the ion ratios described next. At the end of this paper we comment on other features observed in Figure 2 (and Figure 4).

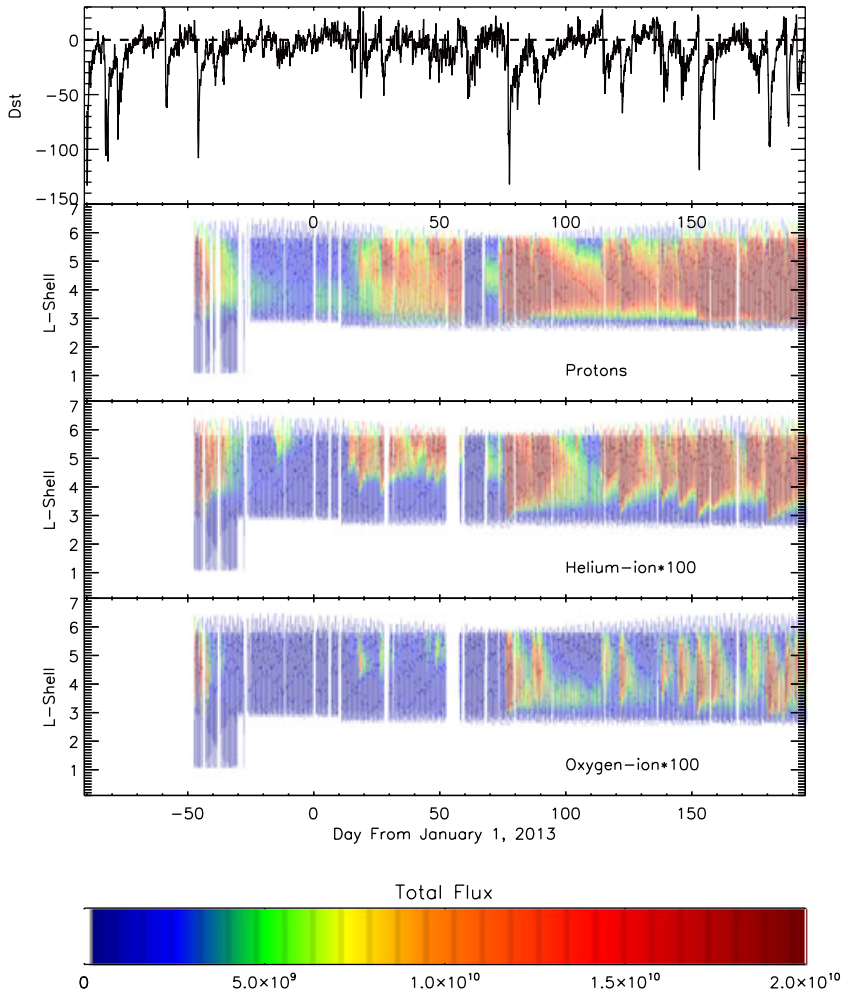

Figure 2. (first panel) Hourly *Dst* values as reported by the World Data Center (WDC) for Geomagnetism, Kyoto, Japan. Time is measured in days from 1 January 2013. (second to fourth panels) H-ion (between the ~45 keV to ~600 keV energy range), He-ion (between the ~65 keV to ~520 keV energy range), and O-ion (between the ~140 keV to ~1130 keV energy range) flux (particles/(s cm^2)), respectively, as measured by the RBSPICE instrument aboard the Van Allan Probes spacecraft B, binned into 30 min, 0.1 L shell realizations. *L* here is determined by a dipole L model. The RBSPICE instrument was shut off below *L* ~3 to reduce anomalous currents and instrument alarming.

In Figure 4 we plot the He/H and the O/H ratios, respectively, along with hourly *Dst*. The ratios are formed using the native energy ranges listed above and are not over a jointly common energy range (i.e., ~140 keV to ~520 keV), in an effort to report total ring current ion abundance. With an energy of 100 keV, the predicted charge exchange lifetimes of H-ions at an L shell of 5 and 3.5 are ~20 days and ~4.5 days, respectively, and are therefore much longer than the predicted/observed charge exchange decay rates of He-ions and O-ions at these energies [*Daglis et al.*, 1999; *Ebihara and Ejiri*, 2003]. Thus, using a ratio of the species abundance with H-ion data can account for any unintended observational bias. The use of the ratios also removes the effect of the neutral concentration profile, allowing one to better address charge exchange lifetimes.

The measurements in Figure 4 show that large increases occur in the abundance of He-ion relative to H-ion and O-ion relative to H-ion in the equatorial magnetosphere at the time of all geomagnetic disturbances as indicated by the *Dst* index. We note that H-ions are still the dominant ion species for the events reported herein. The persistence of the increases in He-ion abundance depends strongly on the *L* value. The persistence is quite limited, on the order of 1 day, at the lower *L* values ($L \sim 3$) and substantially longer, on the order of 10 days, at the highest *L* values ($L \sim 6$). Conversely, the persistence of the increases in O-ion

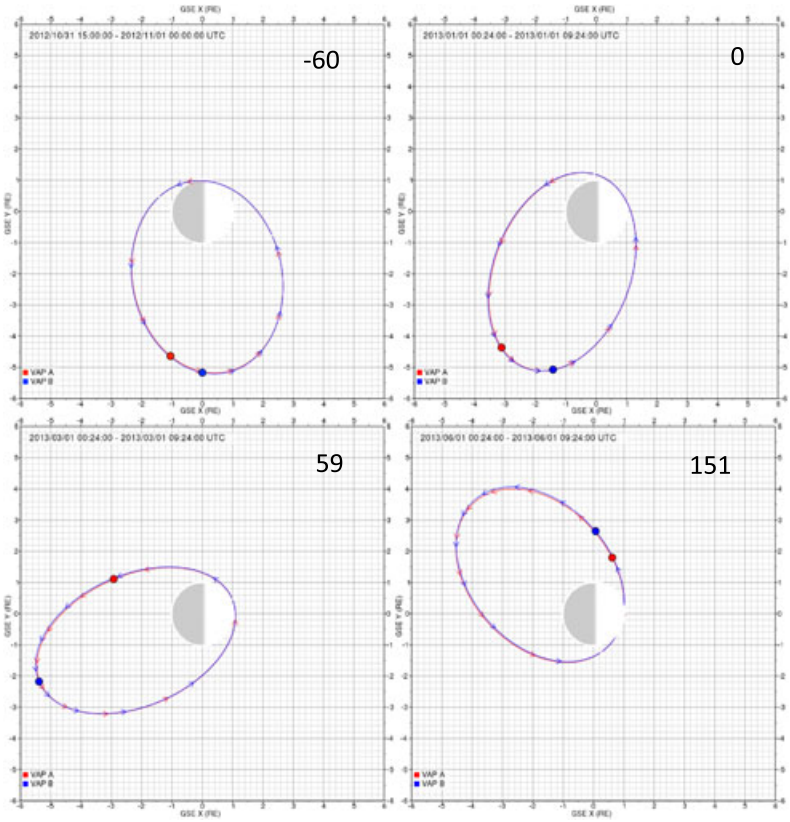

Figure 3. Orbital plots in the GSE *X*-*Y* plane for four sample times spanning Figure 2. Day of year is listed in the upper right-hand corner of each panel.

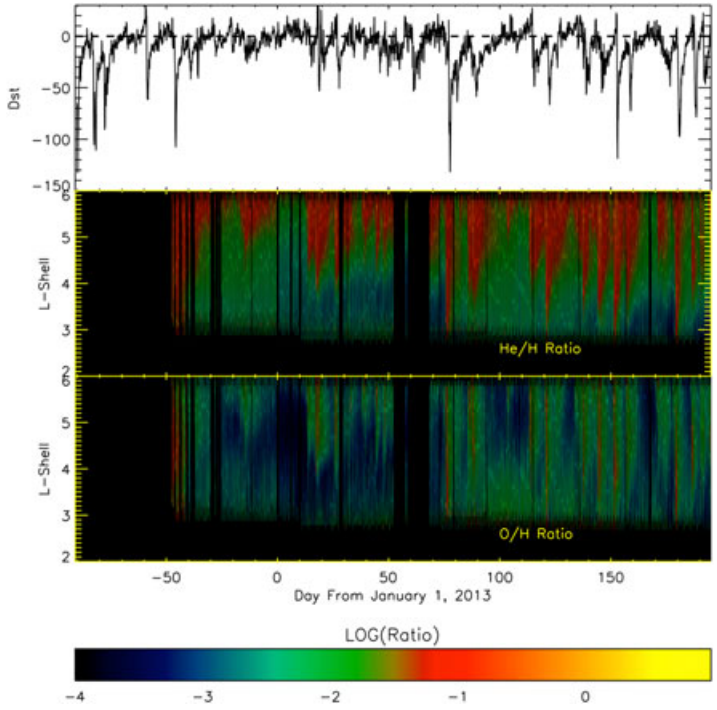

Figure 4. (top) Hourly *Dst* values as reported from the WDC for Geomagnetism, Kyoto, Japan. Time is measured in days from 1 January 2013. *L* here is determined by a dipole L model. (middle) Time/L shell distribution of the He-ion/H-ion ratio. (bottom) Time/L shell distribution of the O-ion/H-ion ratio. Ratios are calculated from the flux values of Figure 2 across the entire energy range of Figure 1.

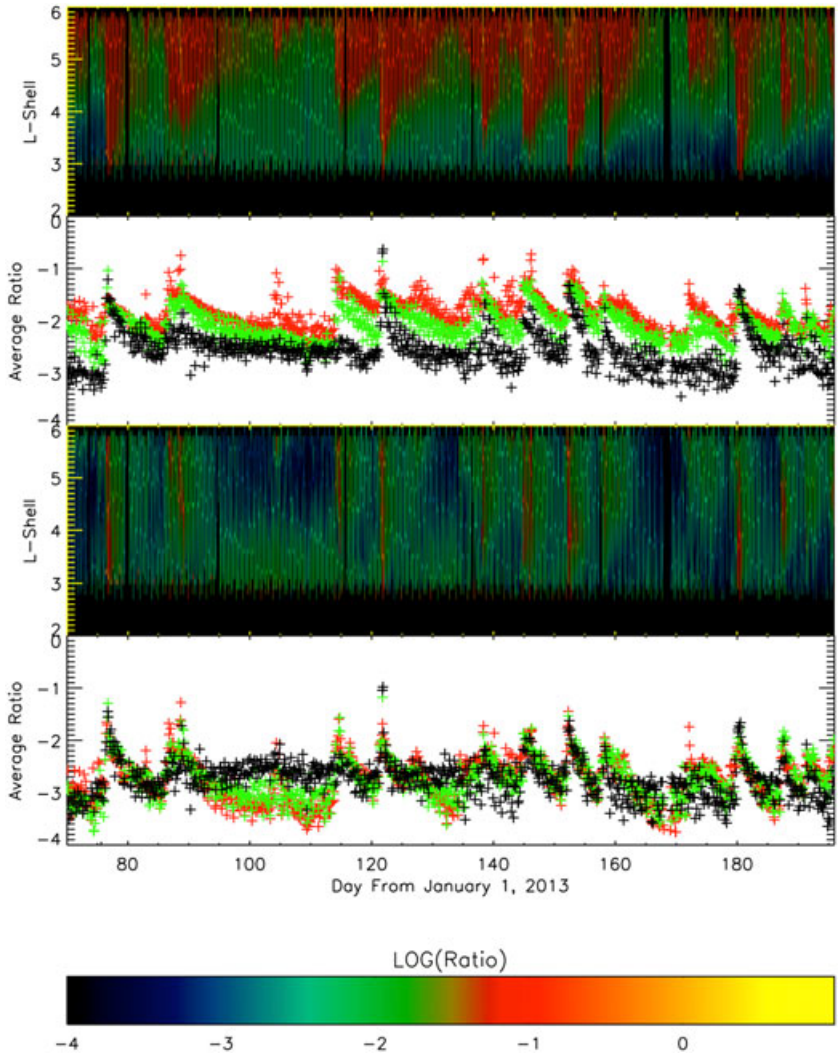

Figure 5. (first and third panels) He-ion/H-ion and O-ion/H-ion ratios across the entire RBSPICE instrument energy ranges, respectively, from Figure 3 but plotted over 2013 day of year (DOY) 70–196. (second and fourth panels) Time traces of the average (log) ratio in three L shell bins; black for L = 3–4, green for L = 4–5, and red for L = 5–6. L here is determined by a dipole L model.

abundance is not associated with L value, as the injection decay, lasting on the order of 1 day, is observed across all L shells equally (Figure 4 (bottom)).

This difference in the persistence of the He-ion and O-ion abundances as a function of L value is quantified in Figure 5 for a sample period of 2013 day of year 70 to 195. In this figure, the values of the He/H and O/H ratios are plotted as a function of time, orbit by orbit, averaged over the ratio values in three L bands: L = 3–4 (black data points), L = 4–5 (green), and L = 5–6 (red). Through exponential fits to 20 injection events, we report that the average decay rate, as determined by the e-folding time, for He-ions in the L = 3–4 band to be ~0.8 days, for He-ions in the L = 4–5 band to be ~1.1 days, and in the L = 5–6 band to be ~1.7 days. Uncertainties on each of these fits are estimated to be ~0.2 days and due to constraints on the initial amplitude and baseline value of the He/H ratio. At the times of increase (times of particle injection) in the relative He-ion abundance, the He/H ratio can reach values between ~5% and 10%. After the decay of the He-ion population relative to the H-ion in this energy band, the He/H ratios at all L values can fall to less than 1%.

This L shell dependence in decay is not observed in the relative O-ion abundance and instead exhibits uniform decay across all L shells. Furthermore, the decay time is quite rapid, occurring with an e-folding time of ~1.5 ± 0.1 h.

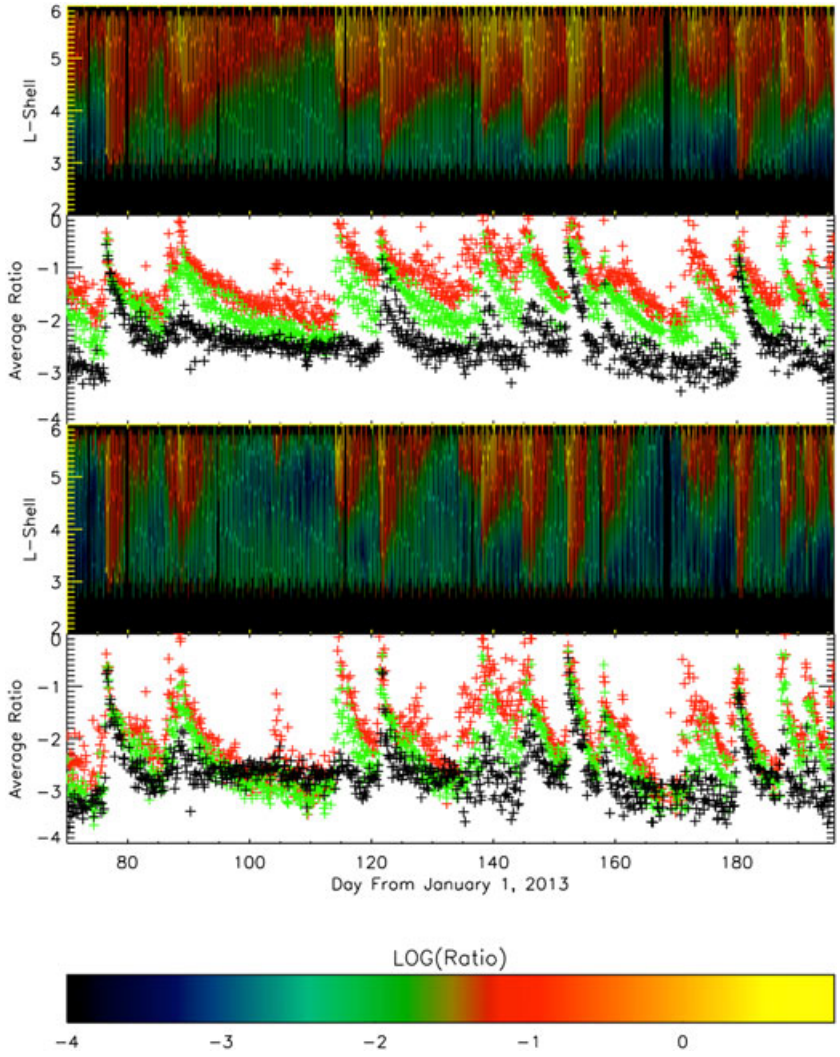

Figure 6. (first and third panels) He-ion/H-ion and O-ion/H-ion ratios across the common RBSPICE instrument energy ranges, respectively, from Figure 3 but plotted over 2013 DOY 70–196. (second and fourth panels) Time traces of the average (log) ratio in three L shell bins; black for L = 3–4, green for L = 4–5, and red for L = 5–6. L here is determined by a dipole L model.

3. Discussions and Conclusions

As indicated in all figures, the H-ion, He-ion, and O-ion abundance and ratio values are correlated with geomagnetic activity, which is consistent with previous observations [e.g., *Kronberg et al.*, 2012]. The use of the "total abundance" values herein are an effort to ascertain the total flux of the ring current species. These values assist in our understanding ring current populations and of ionospheric outflow densities, which are the primary contributor to O-ions during geomagnetic events [*Daglis et al.*, 1999].

We also note our inherent assumption that the loss rate is inferred based on the persistence time of ions after an injection event. It is possible that, however, there are some continued source of heavier ions (particularly at high L) even during the recovery phase. Such additional source material would lend to lengthier decay estimations from the data.

Generally, the L shell dependence of the He-ion and O-ion plasma decay is likely the result of charge exchange loss processes which, due to the falloff of neutral hydrogen density with altitude, causes a loss of the innermost L shells faster than the outermost regions. The measured He-ion lifetimes reported herein seem to support this approach and correspond to previously published lifetime calculations [*Ebihara and*

Ejiri, 2003]. However, the rapid O-ion loss rate is not expected based on our current understanding of O-ion charge exchange.

We suspected such rapid loss in the O-ions was due to the inclusion of the higher-energy (i.e., greater than 500 keV) O-ions in our O/H ratios. In Figure 6 we repeat the same presentation used for Figure 5, but now constrain the ratios such that only the common energy values depicted in Figure 1 are used. With the use of such common energy ranges, the observed O/H ratios now match that of *Ebihara and Ejiri* [2003]. Specifically, O/H *e*-folding decay times were found to be ~0.3 days for the L = 3–4 band , ~0.5 days for the L = 4–5 band, and ~0.8 days for the L = 5–6 band. Thus, it is the rapid loss of high-energy O-ion that gives rise to the extremely short lifetimes apparent in Figure 5. To our knowledge this is the first time that such rapid loss rates associated with high-energy O-ions have been observed. The reason for such fast decay for high-energy O-ions is unclear, but could be due to diffusive or convective outflow processes or perhaps field line curvature scattering [*Ebihara et al.*, 2011]. In addition, we note that the use of common energy ranges also slightly extended the measured He/H lifetimes due to the exclusion of, otherwise faster decaying, lower energy He-ions.

For completeness, we note that there are time periods in which other loss processes seem to be occurring. For example, as seen in Figures 2 and 4, the apparent loss of O-ions around day of year 100, 130, and 165 at higher L shells, before lower L shells, is intriguing. In addition, from the same figures, it is observed that He-ions enter the inner magnetosphere without simultaneous O-ions around day of year −20 and 70. Such an event could be associated with direct coupling of the solar wind without induced terrestrial outflow. Understanding the dynamics of these periods, which perhaps involve wave-particle interaction processes and solar wind conditions, is ongoing and will be explored in future studies. These will incorporate, as required, electric and magnetic field data acquired by Van Allen Probes instruments.

Acknowledgments

The authors thank team discussions with the larger RBSPICE and Van Allan Probes teams. M.G. was supported in part by NSF-AGS-1303646. The RBSPICE instrument was supported by JHU/APL subcontract 937836 to the New Jersey Institute of Technology under NASA prime contract NAS5-01072. All RBSPICE data can be obtained from the RBSPICE SOC at http://rbspice.ftecs.com. Processing code can be obtained from the first author. The *Dst* hourly data came from the World Data Center for Geomagnetism, Kyoto, Japan, at http://wdc.kugi.kyoto-u.ac.jp/dstdir/.

Larry Kepko thanks the reviewers for their assistance in evaluating this paper.

References

Daglis, I. A., E. T. Sarris, and B. Wilken (1993), AMPTE/CCE CHEM observations of the energetic ion population at geosynchronous altitudes, *Ann. Geophys.*, *11*, 685–696.

Daglis, I. A., R. Thorne, W. Baumjohann, and S. Orsini (1999), The terrestrial ring current: Origin, formation, and decay, *Rev. Geophys.*, *37*(4), 407–438, doi:10.1029/1999RG900009.

Ebihara, Y., and M. Ejiri (2003), Numerical simulation of the ring current: Review, *Space Sci. Rev.*, *105*, 377–452.

Ebihara, Y., M.-C. Fok, T. J. Immel, and P. C. Brandt (2011), Rapid decay of storm time ring current due to pitch angle scattering in curved field line, *J. Geophys. Res.*, *116*, A03218, doi:10.1029/2010JA016000.

Fritz, T. A., and S. M. Krimigis (1969), Initial observations of geomagnetically trapped protons and alpha particles with OGO 4, *J. Geophys. Res.*, *74*, 5132–5138.

Fu, S., Q. Zong, Z. Pu, and W. Liu (2003), Effects of geomagnetic and solar activities on the composition and position of the ring current ion, *Chin. J. Geophys.*, *46*(6), 1041–1049.

Fu, S. Y., Q. G. Zong, B. Wilken, and Z. Y. Pu (2001), Temporal and spatial variation of ion composition in the ring current, *Space Sci. Rev.*, *95*, 539–554.

Gloeckler, G., F. M. Ipavich, B. Wilken, W. Stuedemann, and D. Hovestadt (1985), First composition measurement of the bulk of the storm-time ring current (1 to 300 KeV/e) with AMPTE-CCE, *Geophys. Res. Lett.*, *12*, 325–328, doi:10.1029/GL012i005p00325.

Hamilton, D. C., G. Gloeckler, F. M. Ipavich, W. Studemann, B. Wilken, and G. Kremser (1988), Ring current development during the great geomagnetic storm of February 1986, *J. Geophys. Res.*, *93*, 14,343–14,355, doi:10.1029/JA093iA12p14343.

Keika, K., L. M. Kistler, and P. C. Brandt (2013), Energization of O^+ ions in the Earth's inner magnetosphere and the effects on ring current buildup: A review of previous observations and possible mechanisms, *J. Geophys. Res. Space Physics*, *118*, 4441–4464, doi:10.1002/jgra.50371.

Kistler, L. M., F. M. Ipavich, D. C. Hamilton, G. Gloeckler, B. Wilken, G. Kremser, and W. Studemann (1989), Energy-spectra of the major ion species in the ring current during geomagnetic storms, *J. Geophys. Res.*, *94*, 3579–3599, doi:10.1029/JA094iA04p03579.

Konradi, A., D. J. Williams, and T. A. Fritz (1973), Energy-spectra of the major ion species in the ring current during geomagnetic storms, *J. Geophys. Res.*, *78*, 4739–4744, doi:10.1029/JA078i022p04739.

Krimigis, S. M., and J. A. Van Allen (1967), Geomagnetically trapped alpha particles, *J. Geophys. Res.*, *72*, 5779–5797.

Kronberg, E. A., S. E. Haaland, P. W. Daly, E. E. Grigorenko, L. M. Kistler, M. Fränz, and I. Dandouras (2012), Oxygen and hydrogen ion abundance in the near-Earth magnetosphere: Statistical results on the response to the geomagnetic and solar wind activity conditions, *J. Geophys. Res.*, *117*, A12208, doi:10.1029/2012JA018071.

Mauk, B. H., N. J. Fox, S. G. Kanekal, R. L. Kessel, D. G. Sibeck, and A. Ukhorskiy (2012), Science objectives and rationale for the radiation belt storm probes mission, *Space Sci. Rev.*, *179*(1-4), 3–27, doi:10.1007/s11214-012-9908-y.

Mitchell, D., et al. (2013), Radiation Belt Storm Probes Ion Composition Experiment (RBSPICE), *Space Sci. Rev.*, *179*(1-4), 263–308, doi:10.1007/s11214-013-9965-x.

Pulkkinen, T. I., N. Y. Ganushkina, D. N. Baker, N. E. Turner, J. F. Fennell, J. Roeder, T. A. Fritz, M. Grande, B. Kellett, and G. Kettmann (2001), Ring current ion composition during solar minimum and rising solar activity: Polar/CAMMICE/MICS results, *J. Geophys. Res.*, *106*(A9), 19,131–19,147, doi:10.1029/2000JA003036.

Sheldon, R. B., and D. C. Hamilton (1993), Ion transport and loss in the Earth's quiet ring current: 1. Data and standard model, *J. Geophys. Res.*, *98*, 13,491–13,508, doi:10.1029/92JA02869.